2013 IEEE International Conference on Robotics and Automation (ICRA)
Karlsruhe, Germany, May 6-10, 2013

Monocular Feature-Based Periodic Motion Estimation for Surgical Guidance

Stephen Tully, George Kantor, Howie Choset

Abstract— **In this paper, we present a novel approach for mapping periodically moving visual features with a monocular camera. Our target application is the estimation of moving surfaces during minimally invasive surgery for the purpose of aiding in the guidance of surgical tools. Our approach uses a bank of Kalman filters to estimate FFT parameters that encode the periodic motion of visually detected features. To ensure convergent estimation for this highly nonlinear problem, we have developed an iterative update procedure that treats the Kalman filter measurement update step as an optimization problem. Unlike existing solutions that rely on stereo vision, our approach estimates periodic motion with a single moving camera. With an experiment involving a beating heart phantom, we have shown that our approach is able to successfully estimate the periodic motion of visual features.**

I. Introduction

Minimally invasive surgery (MIS) has been shown to reduce patient trauma and shorten hospitalization stays. The impact of MIS has been widespread and has improved patient care, but when operating through a small incision, a surgeon loses the "bird's eye view" that he or she is accustomed to with open surgery. Thus, for guidance during MIS, surgeons must rely on medical imaging, such as fluoroscopy [1], MRI [2], CT [3], and ultrasound [4]. Unfortunately, these imaging modalities either have a limited field-of-view, are incompatible with robots, or emit prolonged radiation.

An alternative approach to surgical guidance is model-based *image-guided surgery*. With image-guidance, patient specific surface models representing the anatomy are generated using preoperative imaging (typically CT or MRI). Then, in real-time during an operation, a computer generated 3D rendered visualization displays the position of magnetically or optically tracked surgical devices relative to the anatomy. The advantage of image-guidance is that the surgeon can rotate the 3D rendered models on the computer screen to gain a better spatial understanding of where the tool or robot is located with respect to an anatomical target.

Thus far, image-guidance solutions have been limited to the use of static 3D anatomical models despite the fact that the anatomy is dynamic due to physiological motion. We believe that a new image-guidance solution is needed that can estimate the periodic motion of nearby organ surfaces in order to better represent the true state of an operation during minimally invasive surgery. The research challenge is to create a convergent filtering algorithm that can accurately estimate parameters that define the physiological motion.

S. Tully, G. Kantor and H. Choset are with the Robotics Institute at Carnegie Mellon University, Pittsburgh, PA 15213, USA, {stully@andrew, kantor@ri, choset@cs}.cmu.edu.
S. Tully is supported by Army Research Office Grant #W911NF1010343.

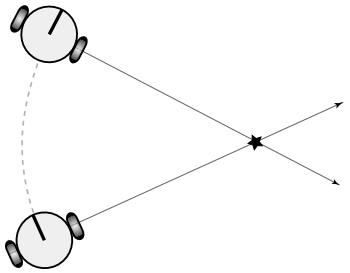

Fig. 1. A conceptual depiction of a robot using parallax to triangulate the location of a sensed feature.

In this paper, we are presenting a solution for the mapping of periodically moving visual features with a monocular camera. This is a new contribution beyond existing solutions that require stereo vision [5]–[7]. Mapping 3D information with monocular vision is possible because a moving camera can view features from different vantage points, exploiting parallax, see Fig. 1. Due to the nonlinearity of this mapping task, the conventionally adopted extended Kalman filter (EKF) is susceptible to divergence. To avoid these issues, we adopt the iterated extended Kalman filter (IEKF) and encode the motion of visually tracked features with FFT parameters.

The main contribution of this work is the introduction of a new approach for estimating physiological motion during image-guided interventions. We note that we are solving a mapping problem, and not a full-fledged simultaneous localization and mapping problem, due to the fact that sufficient localization methods exist for surgical tools (we assume that an electromagnetic or optical tracking solution tracks the camera pose). We believe that our mapping method can have an impact on the accuracy and efficacy of minimally invasive surgery, especially in the case of robotic systems.

II. Background

A. Image-Guided Surgery

Image-guided surgery involves tracking a surgical tool and registering its pose to preoperative images in order to overlay a depiction of the tool on the rendered preoperative models. For example, in [8], Cleary et. al. use an electromagnetic (EM) tracker to guide a tool and register its position with respect to preoperative images. Ensite NavX (St. Jude Medical, St. Paul, MN, USA) and Carto XP/CartoMerge (Biosense Webster, Diamond Bar, CA, USA) are commercial examples of image-guidance that are used for electrophysiology applications. Unfortunately, the majority of existing image-guidance systems rely on static models despite the presence

of complex physiological motion.

B. Monocular Feature Mapping

The monocular simultaneous localization and mapping (SLAM) problem deals with the mapping of visual features with a single camera while localizing a robot. The key to monocular SLAM is that by sensing a feature from different vantage points, the location of features in the world can be mapped via triangulation, see Fig. 1. When approached from a probabilistic standpoint, monocular SLAM is a challenging problem due to the nonlinearity of the camera measurement model [9]. There have been many solutions to counteract the nonlinearity issues of monocular SLAM [10]–[12] including our own solution presented in [9], [13] that uses an iterative algorithm to perform the measurement update step, which is motivated by the work presented in [14]. These monocular SLAM approaches are concerned with the mapping of static features rather than dynamic surface motion.

C. Filtering for Surgery

There has recently been a number of filtering algorithms that have been introduced for surgical estimation. For example, Grasa et. al. [15] use an endoscope to perform SLAM for MIS. The authors rely on the use of an EKF with undelayed initialization of visual landmarks. Similarly, in [16], the authors use a fiberscope with a proximally mounted CCD camera to recover camera motion and 3D scene information during minimally invasive surgery. In [17], the authors estimate the pose of a stereoscope while simultaneously estimating the 3D positions of visually detected features during MIS. These papers have only focused on the mapping of static features for surgical estimation despite the need for a motion-enabled solution that accounts for surface movement.

D. Periodic Motion Estimation

One example of periodic motion estimation in the context of surgery is the work presented in [5]. The authors introduce an algorithm that performs stereo-vision based SLAM within the body while accounting for periodic motion. But unlike the approach that we are presenting, the work in [5] does not use fast Fourier transform (FFT) parameters to encode motion and instead only accounts for a single sinusoidal offset in terms of depth (the dimension orthogonal to the camera). This means that their approach does not account for the complex motion that can occur when organs deform.

In the work by Richa et. al. in [6], [7], a thin-plate spline model is used to to track visually detected periodically moving features in the camera images of a stereo camera. The way that our method extends the work by Richa et. al. is that we are performing monocular estimation rather than stereo estimation. Thus, we believe that our approach is preferable for surgical scopes that are equipped with a single camera sensor. This also means that our approach must deal with the nonlinear filtering issues common to monocular problems (resolving depth through parallax). Another example of periodic motion estimation is presented in [18], in which Bachta et. al. investigate the use of amplitude modulation to predict periodic heart motion.

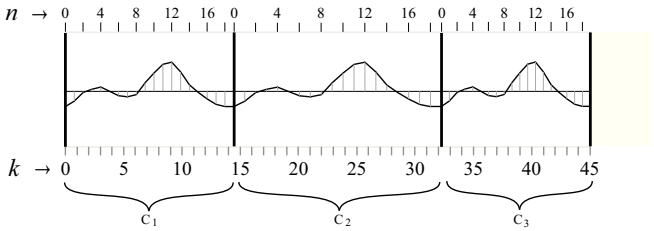

Fig. 2. A depiction of a periodic signal with varying cycle lengths. The index n represents the phase in the current cycle and k is the overall time-step for an experiment. The labels C_1, C_2, and C_3 correspond to each periodic cycle of the experiment.

III. Monocular Periodic Feature Mapping

To perform monocular mapping of periodically moving visually detected features, we have developed a filtering framework that encodes motion with FFT parameters. The problem formulation and our solution are described below.

A. Assumptions

The following is a list of the assumptions that we are making for our periodic motion filtering algorithm. We believe these are reasonable assumptions due to the fact that they do not impose significant restrictions and because there are ways to relax these assumptions with future work.

- **A1:** The pose of the camera is known.
- **A2:** The camera projection models are known.
- **A3:** The signal period phase and duration is known.

We are making assumption **A1** because we have chosen to focus primarily on the mapping aspect of this estimation problem. In addition, we believe **A1** is a safe assumption to make because accurate techniques exist to separately track the pose a surgical device (e.g. EM and optical trackers).

We believe that assumption **A2** is a safe assumption because a calibration procedure can be performed prior to a surgical intervention to determine the camera-specific intrinsic and extrinsic parameters for a fixed-zoom camera. For our experiments we use the Matlab calibration toolbox [19].

We are making assumption **A3** because we believe it is feasible to create a system that inputs an EKG signal (in the case of cardiac motion) to track the phase of the cardiac cycle. In the case of respiratory motion, it may be possible to create a system that tracks the patient's chest displacement. We assume the duration of the period of the signal can be determined by observing the duration of the previous cycle.

B. Periodic Signals

Due to physiological motion, features in the body are moving in a periodic manner. In Fig. 2, we provide an example of a periodically moving signal from cardiac data that has varying cycle lengths. This is the type of signal that would be unknown at the start of an experiment and that we would like to estimate with our filtering algorithm for each cartesian coordinate (x, y, and z) of a moving feature. For this discussion, we can assume that the example in Fig. 2 corresponds to the x-coordinate of a single moving feature.

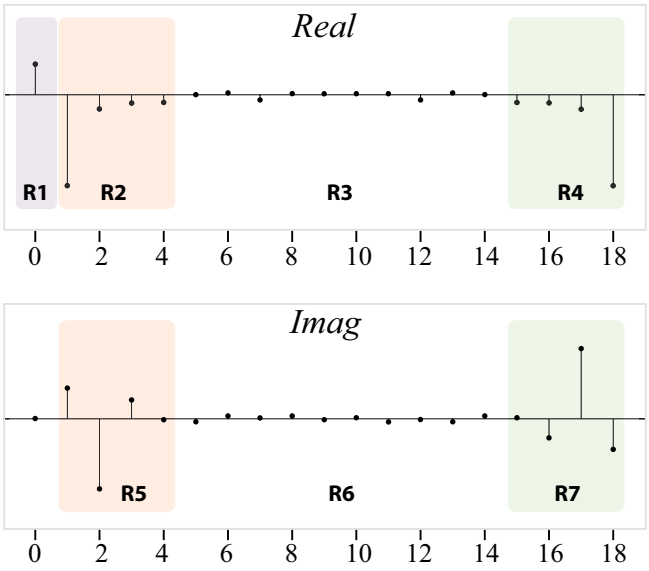

Fig. 3. A depiction of the FFT of a periodic signal. The *real* component is shown (top) and the *imaginary* component is shown (bottom).

The variation in the signal period, during an experiment, may be caused by a varying heart rate or breathing rate. For example, the signal in Fig. 2 has a much longer C_2 cycle in comparison to C_1 and C_3. In Fig. 2, the index n represents the phase in the current periodic cycle and k is the overall time-step for an experiment. Thus, camera measurements are acquired asynchronously with respect to the phase of the cycle. This does not complicate the problem due to the fact that the phase of the periodic cycle is known (assumption **A3**), and thus we can associate a measurement to a phase.

C. Kalman Filter State Vector

To map the periodic motion of visually detected features, our solution is to include dynamic parameters within a Kalman filter mapping algorithm. The parameters that we are using to encode the motion of visual features are fast Fourier transform (FFT) parameters. In Fig. 3, the FFT is shown that corresponds to one period of the signal in Fig. 2. The FFT is comprised of a real part that is symmetric and an imaginary part that is odd-symmetric, assuming real signals.

By looking at the example FFT in Fig. 3, it is apparent which parameters capture the motion of the underlying signal. From the real part, we include the parameters within regions **R1** and **R2** in our Kalman filter state vector. Likewise, from the imaginary part, we include the parameters within region **R5** in our Kalman filter state vector. In Fig. 3, the parameter within region **R1** represents the DC or zero-frequency component of the FFT. This parameter defines the mean of the motion path for whatever coordinate this signal corresponds to (x, y, or z). It is worth noting that the regions **R3**, **R4**, **R6**, and **R7** are not included in the Kalman state vector. This is because the coefficients are either negligible or redundant due to the inherent symmetry of the FFT.

Based on the above analysis of the FFT for typical physiological motion, we can formulate the Kalman filter state vector as follows,

$$\mathbf{x}_k = \begin{bmatrix} x_{DC} & y_{DC} & z_{DC} & \mathbf{f}_x{}^T & \mathbf{f}_y{}^T & \mathbf{f}_z{}^T \end{bmatrix}^T.$$

This state vector includes the DC terms of the periodic motion (x_{DC}, y_{DC}, and z_{DC}), and three vectors containing the FFT parameters (as discussed above), which are represented by ($\mathbf{f}_x$, $\mathbf{f}_y$, and $\mathbf{f}_z$). We note that our discussion of Fig. 3 is simply an example: thus, the number of FFT parameters included in the state vector may be chosen by the user.

D. Filter Prediction Step

The position of a feature at any given point in time, according to our Kalman filter formulation, is completely determined by the state vector $\mathbf{x}_k$ along with the phase of the periodic cycle. For this reason, despite the fact that there is inherent motion in the position of a feature, there is no "motion" of the state vector parameters. Thus, we can define the Kalman filter prediction step as follows,

$$\mathbf{x}_{k+1} = f(\mathbf{x}_k) = \mathbf{x}_k.$$

The implication of this is that our filtering algorithm is only dependent upon the implementation of a Kalman measurement update step (the prediction step is simply ignored).

IV. Iterative Update for Periodic Estimation

In Sec. III, we discussed how our Kalman filter formulation seeks to estimate a state vector (one per visually detected feature) that includes FFT parameters for reconstructing the motion. To review, the main idea is to estimate a Kalman state vector that is initially unknown by applying camera observations. Then, when the parameters of the FFT are accurately estimated by the Kalman filter for a given feature, its spatial motion can be recovered by computing the inverse-FFT for each cartesian component (x, y, and z). In this section, we will present our iterative Kalman measurement update step for applying camera observations.

A. Monocular Measurement Model

The monocular measurement model of a point feature with a cartesian (x, y, z) representation can be written as follows,

$$\mathbf{h}(\mathbf{x}_k) = \begin{bmatrix} \text{atan2}(y - y_R, x - x_R) \\ \text{atan2}(z - z_R, \sqrt{(x - x_R)^2 + (y - y_R)^2}) \end{bmatrix}, \quad (1)$$

where (x_R, y_R, z_R) is the position of the robot or camera in the world. This models the mapping of a feature position to the feature bearing-angles relative to the coordinate frame of the camera. We note that an alternate model that could be used without significantly changing the method is a (x, y, z) projection to the pixel location (u, v) in the camera image.

The measurement model of the Kalman filter computes the expected bearing-angle measurements given a state vector $\mathbf{x}_k$. To implement the measurement function given our unconventional Kalman state vector with FFT parameters, we must first reconstruct, from $\mathbf{x}_k$, the full FFT that corresponds to the periodic motion of the feature. This involves filling in zeros for the elements of the FFT that we chose not to encode in the filter and it involves using the known redundancy of

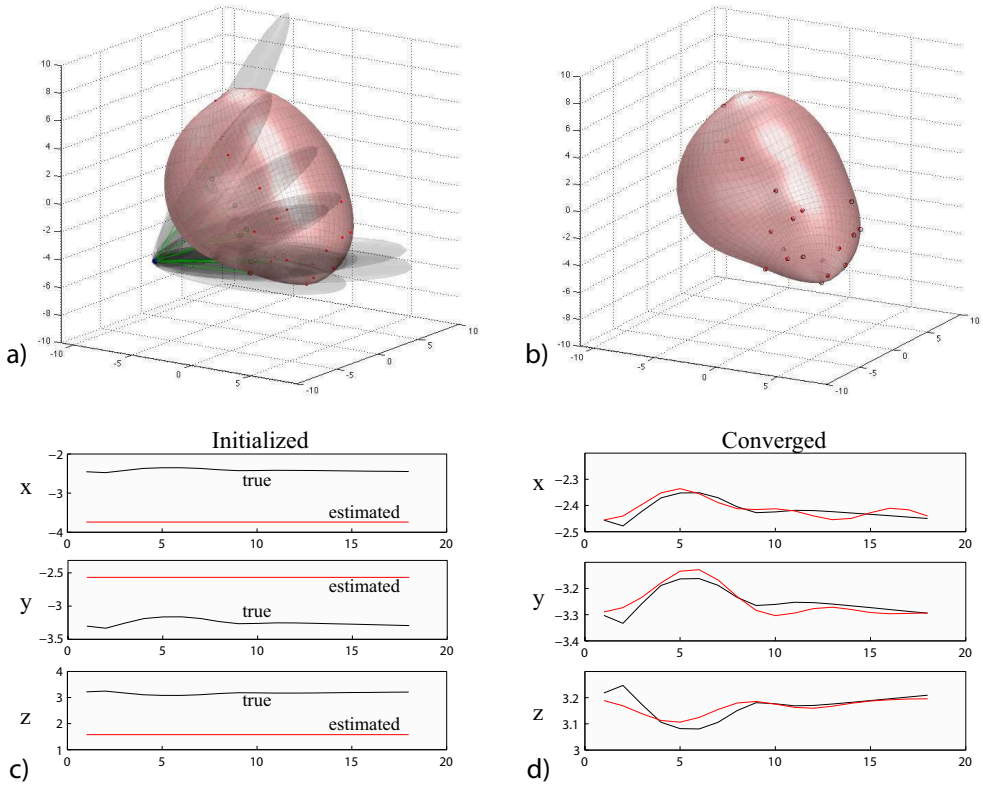

Fig. 4. Experiment I involves a beating heart simulation. In (a), feature initialization is shown, in (b), the result is shown after the estimation of features has converged, in (c), an example cycle is shown upon initialization, and in (d), the same cycle is shown after the algorithm successfully mapped the periodic motion.

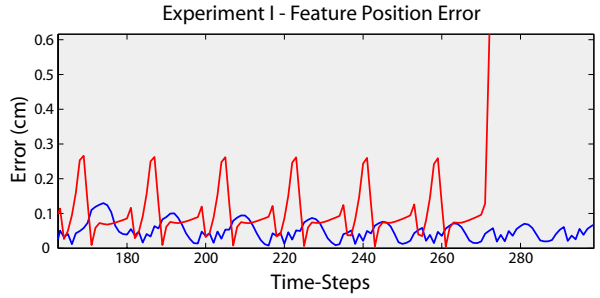

Fig. 5. Experiment I: the error between the estimated position of a moving feature vs ground truth. For static estimation (red), the estimate diverges. For our dynamic solution (blue), the algorithm successfully maps the motion.

the FFT to fill in the additional missing parameters. In other words, with only a few of the FFT parameters represented in the estimated Kalman state vector, we can almost completely reconstruct the FFT. The significance of this is that we can maintain a low dimensionality for the filtering task. We will use the following equations to signify the reconstruction of the FFT that corresponds to the feature motion,

$$\begin{aligned} \mathbf{F}_x &= \text{Reconstruct\_FFT}(\mathbf{f}_x, x_{DC}), \\ \mathbf{F}_y &= \text{Reconstruct\_FFT}(\mathbf{f}_y, y_{DC}), \\ \mathbf{F}_z &= \text{Reconstruct\_FFT}(\mathbf{f}_z, z_{DC}). \end{aligned}$$

After reconstructing the FFT for each component (x, y, and z), we can compute the time-domain signal for the feature motion by using the inverse FFT. Then, we can extract the specific (x, y, z) position of the feature by knowing the phase in the cycle corresponding to the measurement,

$$\begin{aligned} \mathbf{x} &= \mathcal{F}^{-1}(\mathbf{F}_x), \quad x = \mathbf{x}[n] \\ \mathbf{y} &= \mathcal{F}^{-1}(\mathbf{F}_y), \quad y = \mathbf{y}[n] \\ \mathbf{z} &= \mathcal{F}^{-1}(\mathbf{F}_z), \quad z = \mathbf{z}[n]. \end{aligned}$$

The measurement function can then be computed using the monocular measurement model $\mathbf{h}(\mathbf{x}_k)$ from Eq. 1, except, for our definition of the Kalman state vector, the terms extracted from the inverse FFT are used in place of the directly estimated (x, y, z) parameters.

B. Iterative Measurement Update

The conventional extended Kalman filter (EKF) measurement update is the most widely used method for applying sensor measurements to correct a Kalman filter state estimate. Unfortunately, as we have shown in our previous work [9], the EKF is susceptible to a diverging state estimate when applied to monocular mapping problems. To prevent divergence, we have developed an iterative measurement update method. Based on the underlying objective of the Kalman filter to maximize the posterior probability, we can optimize the following cost function,

$$\begin{aligned} \hat{\mathbf{x}}_{k|k} = \arg\min_{\mathbf{x}_k} [&(\mathbf{x}_k - \hat{\mathbf{x}}_{k|k-1})^T \mathbf{P}_{k|k-1}^{-1} (\mathbf{x}_k - \hat{\mathbf{x}}_{k|k-1}) + \\ &(\mathbf{z}_k - \mathbf{h}(\mathbf{x}_k))^T \mathbf{R}^{-1} (\mathbf{z}_k - \mathbf{h}(\mathbf{x}_k))], \end{aligned}$$

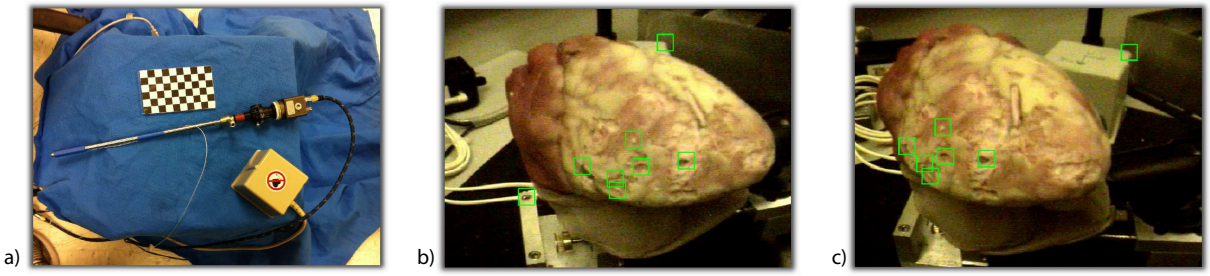

Fig. 6. Experiment II: a photo of the calibration setup is shown in (a), which includes a laparoscope with a camera and a magnetic tracking system. In (b), the rubber heart phantom is shown with acquired tracked features, and in (c), a second image is shown after the camera has moved significantly.

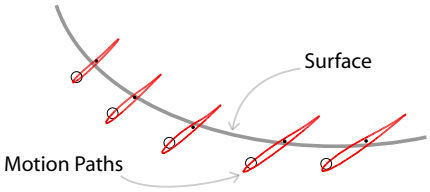

Fig. 7. Experiment II: a birds-eye view of the mapped features. The features are shown as points with a surrounding path defining their periodic motion. The mapped motion paths agree with each other and with the surface motion of the phantom, suggesting that the surface was mapped accurately.

where $\hat{\mathbf{x}}_{k|k-1}$ is the current estimate of the state vector, $\mathbf{P}_{k|k-1}$ is the estimated covariance matrix for the state, and $\mathbf{z}_k$ is a camera measurement corresponding to a feature observed at time-step k. Also, in this cost function, $\mathbf{h}(\mathbf{x}_k)$ is the measurement model (discussed above) and $\mathbf{R}$ is the covariance matrix for the measurement that defines the expected camera sensor noise. The objective of our approach is to replace the current Kalman state vector estimate with the optimal solution to this minimization problem. By applying Gauss-Newton's method to the optimization problem, we have derived the following iterative solution,

$$\begin{aligned}
\mathbf{x}_0 &= \hat{\mathbf{x}}_{k|k-1} \\
\mathbf{K}_i &= \mathbf{P}_{k|k-1}\mathbf{H}_i^T[\mathbf{H}_i\mathbf{P}_{k|k-1}\mathbf{H}_i^T + \mathbf{R}]^{-1} \\
\mathbf{x}_{i+1} &= \mathbf{x}_i + \gamma_i(\mathbf{H}_i^T\mathbf{R}^{-1}\mathbf{H}_i + \mathbf{P}_{k|k-1})^{-1} \\
&* \quad (\mathbf{H}_i^T\mathbf{R}^{-1}(\mathbf{z}_k - \mathbf{h}(\mathbf{x}_i)) + \mathbf{P}_{k|k-1}^{-1}(\hat{\mathbf{x}}_{k|k-1} - \mathbf{x}_i)),
\end{aligned}$$

where $\mathbf{H}_i$ is the Jacobian of the measurement function evaluated at the estimate $\mathbf{x}_i$ and γ_i is a variable step factor. This iterative procedure can be run for a user-defined number of iterations or it can be run until convergence. The new updated estimate $\hat{\mathbf{x}}_{k|k}$ is then set equal to the final solution $\mathbf{x}_i$ after iteration is complete.

V. Experimental Evaluation

A. Experiment I

To validate our FFT-based periodic motion estimation algorithm, we tested the approach on two experimental datasets. The first is primarily a simulation, although the motion data is derived from real gated MRI scans of a human heart [20]. A picture of the simulation is shown in Fig. 4-(a). We simulated a camera in Matlab that traveled a fixed path around the moving cardiac model and we simulated the detection of visual features, with known data association, on all sides of the beating heart. For each bearing-angle measurement that was simulated, artificial noise was added. At the start of the simulation, the estimates of the features, upon initialization, are shown in Fig. 4-(a). The features are shown with large corresponding ellipsoids due to the initial uncertainty of the feature locations and motion parameters.

The result of this experiment is the successful mapping of periodically moving features located on the surface of the heart. When compared to an EKF implemented with the same Fourier series parameterization, the iterated algorithm that we have developed outperformed the EKF. The EKF was prone to divergence after the simulation had progressed. The simulation with mapped features is shown in Fig. 4-(b). An example of one of the features converging to the true motion is shown in Fig. 4-(d). Lastly, a closer look at the performance of our filter is shown in Fig. 5. In this image, the error between the estimated motion path and the true path is plotted over time. For an EKF using only static parameters, the error is more significant due to divergence.

B. Experiment II

Experiment II involves a recorded dataset captured from a laparoscope (shown in Fig. 6-(a)). The moving surface for this trial was a beating heart phantom, shown in Fig. 6-(b) and 6-(c). The phantom beats according to oscillations that are induced by a pneumatic pump. We tracked the pose of the laparoscope with an Ascension Trakstar EM tracking system (Ascension Technologies, Milton, VT, USA). The tracking sensor has an RMS error of 1.4mm. The checkerboard seen in Fig. 6-(a) was used for camera calibration.

For this experiment, we captured 550 camera images of the beating heart phantom. Eight periodically moving visual features were tracked using conventional visual template tracking [21]. The tracked features can be seen in Fig. 6-(b) and Fig. 6-(c). For this experiment, the implementation only required one iteration of the iterative filter for stable estimation. Also, for this experiment, we used the form of the measurement model that projects a feature to a (u,v) pixel location, as opposed to bearing-angles.

In Fig. 7, we show the resulting motion paths that were mapped during Experiment II. The image can be interpreted as a "bird's eye view" of the mapped feature motion. The

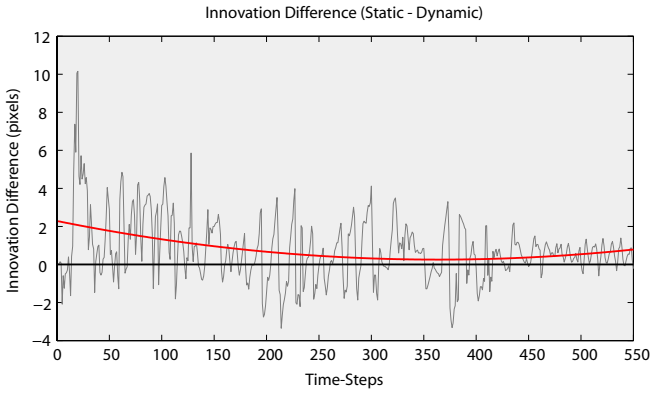

Fig. 8. The difference in the measurement innovation for static estimation and dynamic estimation. Larger (positive) values correspond to our dynamic method outperforming a purely static mapping method. Because this difference is noisy, we have included a best-fit curve (in red).

qualitative result is that the motion paths agree with the expected motion of the surface in that they are moving approximately 3mm in the direction orthogonal to the camera pose. Additionally, the feature motion paths agree with each other, which suggests that the motion was accurately mapped.

A quantitative result for this experiment is shown in Fig. 8, where we plot the *innovation difference* (ID), which is the difference between the innovation for an implementation assuming static features and our implementation with dynamic features. The innovation is the error between the expected measurement (given the measurement model) and the actual measurement that is acquired from the camera. The ID being mostly positive (noisy gray plot in Fig. 8) demonstrates that there is greater error for the static case, thus our motion-enabled feature mapping algorithm outperforms the purely static method. To better visualize the ID, we additionally show a best-fit curve for the ID (shown in red).

VI. Conclusions and Discussion

In this paper, we present a novel approach for mapping periodically moving visual features with a monocular camera. The application is the estimation of moving surfaces during minimally invasive surgery for the purpose of aiding in the guidance of surgical tools. Our approach uses a Kalman filter with FFT parameters and an iterative measurement update step. We have extended periodic motion mapping beyond existing solutions that rely on stereo vision and have shown that our approach can accurately map moving surfaces. We note that we are solving a mapping problem, and not a full-fledged simultaneous localization and mapping (SLAM) problem, due to the fact that sufficient localization methods exist for surgical tools (electromagnetic and optical tracking).

The main contribution of this work is the introduction of a new approach for estimating physiological motion with a monocular camera. We believe our algorithm can have a significant impact on the development of new image-guidance systems for MIS. In particular, we believe that a robot that is aware of the surrounding physiological motion can be better equipped to compensate for such motion.

Acknowledgments

The authors would like to thank Nathan Wood for his assistance with bench-top experiments.

References

[1] L. Joskowicz, M. Sati, and L. Nolte, "Fluoroscopy-based navigation in computer-aided orthopaedic surgery," in *Proceedings of the IFAC Conference on Mechatronic Systems*, 2000.

[2] R. Omary, J. Green, B. Schirf, Y. Li, J. Finn, and D. Li, "Real-time magnetic resonance imaging-guided coronary catheterization in swine," *Circulation*, vol. 107, no. 21, pp. 2656–2659, 2003.

[3] R. Manzke, V. Reddy, S. Dalal, A. Hanekamp, V. Rasche, and R. Chan, "Intra-operative volume imaging of the left atrium and pulmonary veins with rotational x-ray angiography," in *Medical Image Computing and Computer-Assisted Intervention (MICCAI)*, 2006, pp. 604–611.

[4] W. Zhang, R. Rohling, and D. Pai, "Surface extraction with a three-dimensional freehand ultrasound system," *Ultrasound in Medicine and Biology*, vol. 30, no. 11, pp. 1461–1473, 2004.

[5] P. Mountney and G. Z. Yang, "Motion compensated SLAM for image guided surgery," in *Medical Image Computing and Computer-Assisted Intervention (MICCAI)*, 2010.

[6] R. Richa, P. Poignet, and C. Liu, "Efficient 3D tracking for motion compensation in beating heart surgery," in *Medical Image Computing and Computer-Assisted Intervention*, 2008, vol. 5242, pp. 684–691.

[7] ——, "Three-dimensional motion tracking for beating heart surgery using a thin-plate spline deformable model," *The International Journal of Robotics Research*, vol. 29, no. 2-3, pp. 218–230, 2010.

[8] K. Cleary, H. Zhang, N. Glossop, E. Levy, B. Wood, and F. Banovac, "Electromagnetic tracking for image-guided abdominal procedures: Overall system and technical issues," in *Proceedings of the IEEE Int. Conf. on Engineering in Medicine and Biology Society (EMBS)*, 2005.

[9] S. Tully, H. Moon, G. Kantor, and H. Choset, "Iterated filters for bearing-only SLAM," in *Proceedings of the IEEE International Conference on Robotics and Automation (ICRA)*, May 2008.

[10] A. Davison, "Real time simultaneous localisation and mapping with a single camera," in *Proceedings of the International Conference on Computer Vision (ICCV)*, July 2003.

[11] N. Kwok, G. Dissanayake, and Q. Ha, "Bearing-only SLAM using a SPRT based Gaussian sum filter," in *Proceedings of the IEEE International Conf. on Robotics and Automation (ICRA)*, April 2005.

[12] J. Civera, A. Davison, and J. Montiel, "Inverse depth to depth conversion for monocular SLAM," in *Proceedings of the IEEE International Conference on Robotics and Automation (ICRA)*, April 2007.

[13] S. Tully, G. Kantor, and H. Choset, "A single-step maximum a posteriori update for bearing-only SLAM," in *Proceedings of the 2010 AAAI Conference on Artificial Intelligence*, July 2010.

[14] B. Bell and F. Cathey, "The iterated Kalman filter update as a Gauss-Newton method," *IEEE Transactions on Automatic Control*, vol. 38, no. 2, pp. 294–297, 1993.

[15] O. G. Grasa, J. Civera, A. Guemes, V. Munoz, and J. Montiel, "EKF monocular SLAM 3D modeling, measuring and augmented reality from endoscope image sequence," in *Medical Image Computing and Computer-Assisted Intervention (MICCAI)*, 2009.

[16] D. Noonan, P. Mountney, D. Elson, A. Darzi, and G. Z. Yang, "A stereoscopic fibroscope for camera motion and 3D depth recovery during minimally invasive surgery," in *Proceedings of the IEEE International Conference on Robotics and Automation (ICRA)*, 2009.

[17] P. Mountney, D. Stoyanov, A. Davison, and G. Z. Yang, "Simultaneous stereoscope localization and soft-tissue mapping for minimal invasive surgery," in *Medical Image Computing and Computer-Assisted Intervention (MICCAI)*, 2006.

[18] W. Bachta, P. Renaud, L. Cuvillon, E. Laroche, A. Forgione, and J. Gangloff, "Motion prediction for computer-assisted beating heart surgery," *Biomedical Engineering, IEEE Transactions on*, vol. 56, no. 11, pp. 2551–2563, 2009.

[19] Z. Zhang, "A flexible new technique for camera calibration," *Pattern Analysis and Machine Intelligence, IEEE Transactions on*, vol. 22, no. 11, pp. 1330–1334, November 2000.

[20] S. Malchenko and J. Vedru, "Model of heart shape cyclic variation for foucault cardiography simulations," *International Journal of Bioelectromagnetism*, vol. 5, no. 1, pp. 318–319, 2003.

[21] B. Lucas, T. Kanade *et al.*, "An iterative image registration technique with an application to stereo vision," in *Proceedings of the 7th international joint conference on Artificial intelligence*, 1981.